Journal of Environmental Radioactivity 220–221 (2020) 106302

Contents lists available at ScienceDirect

Journal of Environmental Radioactivity

journal homepage: http://www.elsevier.com/locate/jenvrad

Adaptation of the RODOS system for analysis of possible sources of Ru-106 detected in 2017

Ivan V. Kovalets [a,b,*], Oleksandr Romanenko [c], Roman Synkevych [a]

[a] Institute of Mathematical Machines & Systems Problems, NAS of Ukraine, Prosp. Glushkova, 42, 03187, Kyiv, Ukraine
[b] Ukrainian Center of Environmental & Water Projects, Prosp. Glushkova, 42, 03187, Kyiv, Ukraine
[c] Rivne Nuclear Power Plant, National Nuclear Energy Generating Company "Energoatom", 34400, Rivne Oblast, Ukraine

ARTICLE INFO

Keywords:
Source term estimation
Atmospheric dispersion
RODOS
JRODOS
Ru-106
Ruthenium

ABSTRACT

In this work, we present a method to use the European nuclear emergency response system RODOS for analysis of potential sources of airborne radioactivity of an unknown origin. The method is based on a solution of adjoint equations, without modification of the code of long-range atmospheric dispersion model MATCH used in RODOS. The method has been successfully applied to the Ru-106 accident of 2017. The obtained spatial distribution of the correlation between simulations and measurements which could be achieved with source located in a given place, is in a qualitative agreement with analogous results published in other works. The high correlation is centered on the Ural Mountains; this is explained by a very wide expansion of the plume. However, the location of the maximum correlation obtained in this work is in the northern part of Russia, close to a military test site on Novaya Zemlya. This location is far away from the reprocessing plant Mayak in the South-Eastern Urals mentioned in other investigations as the most probable location of the source. In the results presented here, the correlation at the source location corresponding to the Mayak plant is still quite high (0.49); release inventory from this source of about 300 TBq could explain the observed measurements.

1. Introduction

In late September - early October 2017, European and other stations reported detection of ruthenium-106 (Masson et al., 2019). The detected cloud was very large, it covered a big part of Eurasia from Norway to Kuwait and from Germany to East Siberia (Fig. 1). The source of this radionuclide was unclear. At the time of the accident, the International Atomic Energy Agency (IAEA) collected measurements from many countries (IAEA, 2017) and coordinated exchange of information between them. Immediately after the accident, several research teams looked for a potential source of the Ru-106 using mathematical simulations (Kovalets, 2017; Kovalets and Romanenko, 2017; Sørensen, 2018; Saunier et al., 2019; Hamburger and Gering, 2019; Bossew et al., 2019).

The EU nuclear emergency response system RODOS is a software tool designed for forecasting atmospheric transport of radionuclides from a local to planetary scale (Landman et al., 2014a). It is used in many countries in Europe, and it was widely applied to forecast consequences of different radiological accidents such as Fukushima and others (Landman et al., 2014b). However, this system does not include software tools for inverse transport simulations, such as backward trajectories analysis or adjoint equations solving to identify unknown sources of radioactive contamination. Despite this, it is possibile to use RODOS for identification of unknown sources. It was used in several studies identifying contamination sources. In particular, one of the first simulation results showing the map of potential sources of the Ru-106 accident in 2017 was obtained with the RODOS system (Kovalets, 2017; Kovalets and Romanenko, 2017; Hamburger and Gering, 2019). In this work, we describe the approach of solving adjoint equations with the RODOS system (without modifying its source code) and subsequently solving the source identification (or inverse) problem. We describe results of application of this approach to the analysis of possible sources of Ru-106 detected in 2017.

2. Method of source term identification with RODOS

In this work, we use the redesigned Java-version of the RODOS system – JRODOS (Ievdin et al., 2010) that among others contains the long-range Eulerian atmospheric transport model (ATM) MATCH (Robertson and Langner, 1999; Robertson, 2010). Kovalets et al. (2014)

* Corresponding author. Institute of Mathematical Machines & Systems Problems, NAS of Ukraine, prosp. Glushkova, 42, 03187, Kyiv, Ukraine.
E-mail address: ik@env.com.ua (I.V. Kovalets).

https://doi.org/10.1016/j.jenvrad.2020.106302
Received 6 March 2020; Received in revised form 28 April 2020; Accepted 5 May 2020
0265-931X/© 2020 Elsevier Ltd. All rights reserved.

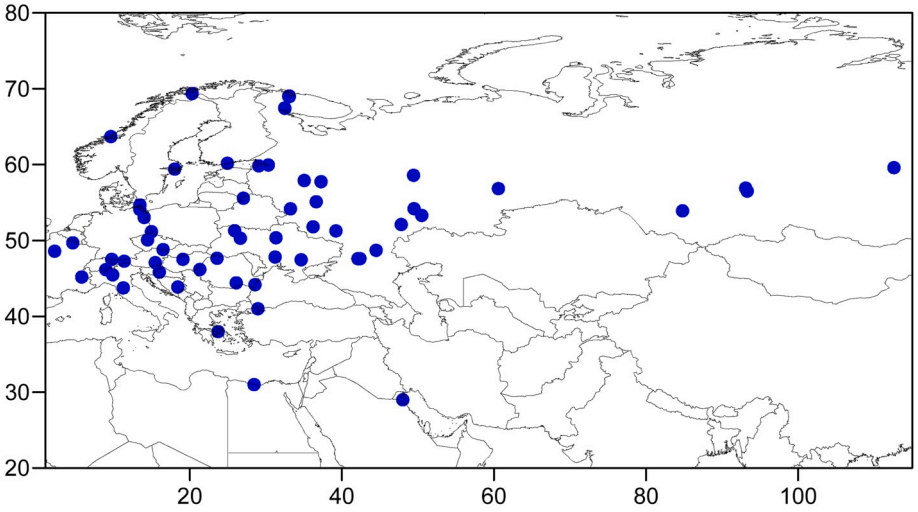

Fig. 1. Map of locations of measurements of Ru-106 used in this study.

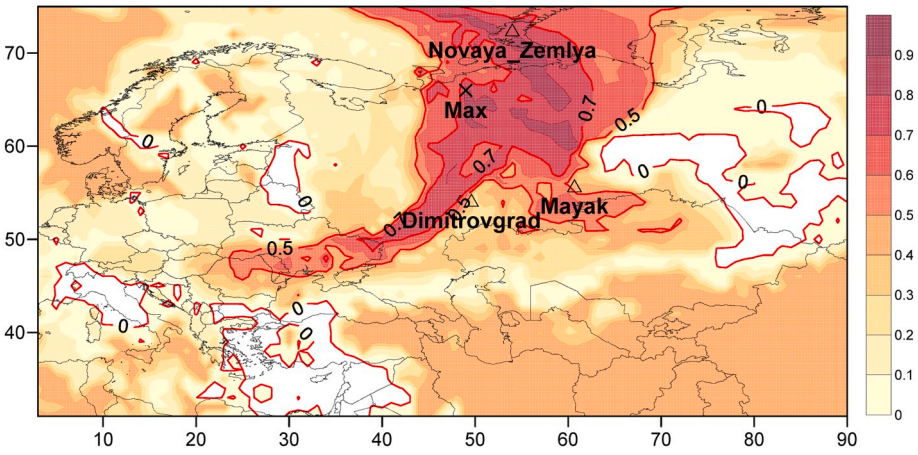

Fig. 2. Spatial distribution of maximum correlation between simulated and observed Ru-106 concentrations for a specific location of the potential source.

developed software tools that enabled MATCH to run on the global meteorological data of the Global Forecasting System (GFS) operated by the US National Center of Environmental Prediction (NCEP), which are freely available in the Internet (NCEP, 2000). In this work, we use this JRODOS-MATCH model for solving forward and backward atmospheric transport problem.

2.1. Formulation of the cost function

Usually the problem of source term identification (source inversion) is formulated as the problem of minimising quadratic cost function of difference between simulated and observed concentrations (Enting, 2002). However, Kovalets et al. (2018) successfully used the correlation-based cost function to estimate location and timing of a finite duration constant-rate release in an urban environment. The solution of the source inversion problem with the correlation-based cost function does not depend on a particular value of the constant release rate and therefore the number of the unknowns is reduced. Although the planetary-scale problem of Ru-106 dispersion in 2017 is very different from the problem considered by Kovalets et al. (2018) and the release rate in our case is certainly not constant, in this work, we use the same correlation-based cost function:

$$J = -\frac{\overline{(c_m - \overline{c}_m)(c_o - \overline{c}_o)}}{\sqrt{\overline{(c_m - \overline{c}_m)^2}}\sqrt{\overline{(c_o - \overline{c}_o)^2}}} \rightarrow_{\psi} \min, \quad (1)$$

where c is concentration, indices 'm' and 'o' denote model and observations respectively, the overline denotes averaging over all measurements used in the source term estimation, i.e. averaging over both time and space.

The cost function J is to be minimised with respect to the control vector ψ that may consist of unknown geographical coordinates of the source x_s, y_s[dec. deg.], time start and duration of the release t_s, δ_s: $\psi = (x_s, y_s, t_s, \delta_s)$. The unknown release rate q_s[Bq·s^{-1}] is constant in this work; therefore, the cost function (1) does not depend on it. The choice of the cost function and the assumption of the constant release rate are justified by research in (Kovalets et al., 2014), which considered RODOS-MATCH simulation of planetary-scale atmospheric transport following the Fukushima accident. In that research, it was demonstrated that while the correlation coefficient of model-predicted plume arrival time obtained with a full time dependent release rate was very good (0.91), the correlation coefficient with a much more crude assumption of a constant in time release rate during the period of maximum releases from Fukushima NPP was still acceptable (0.79). Therefore, in a planetary-scale problem, when most measurements are far from the source, we can hope that the assumption of a constant in time finite duration release will not result in large solution errors.

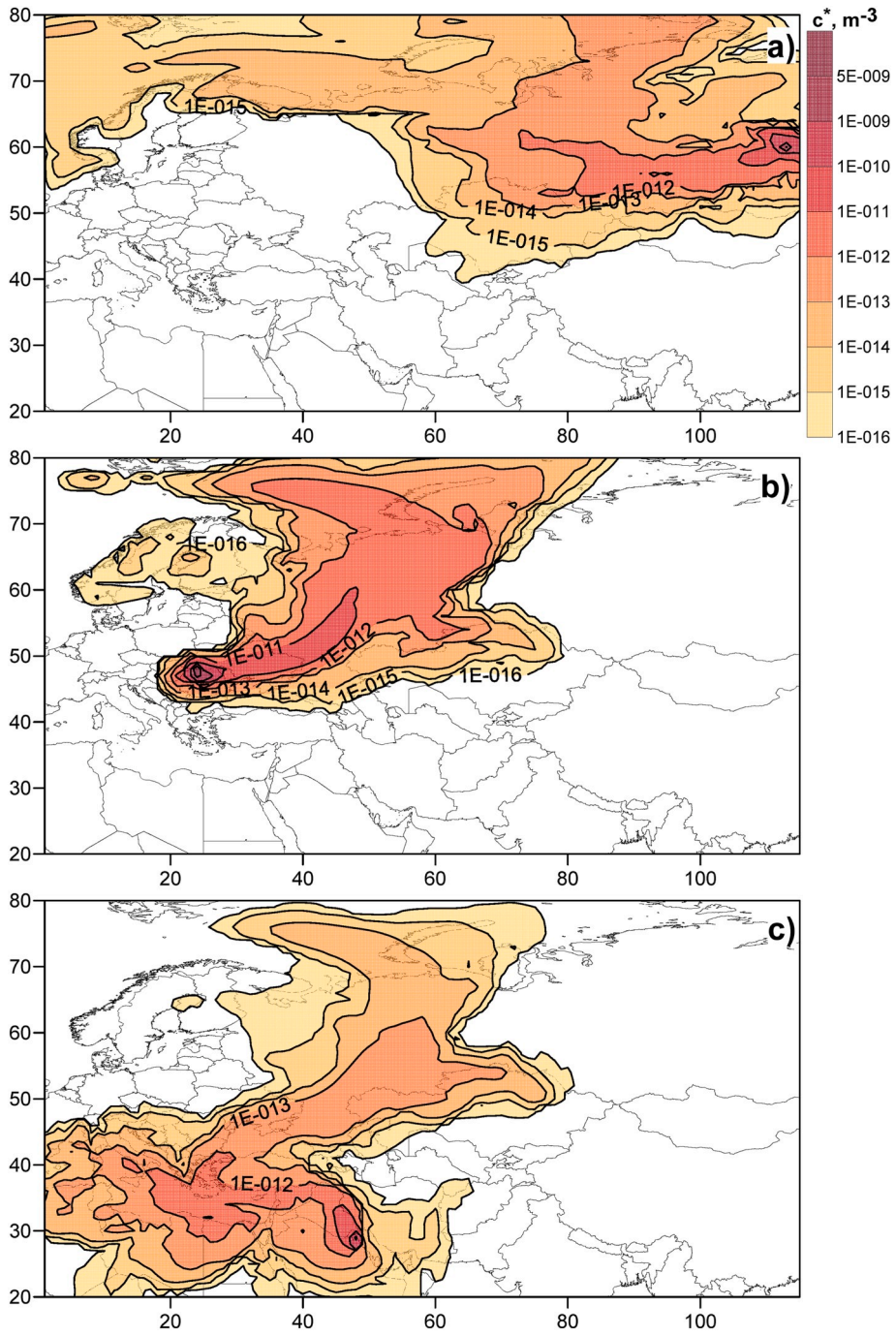

Fig. 3. Spatial distribution of time-averaged adjoint variable: a) backward run from Peleduj, Russia, measurement taken during Oct. 05, 2017; b) backward run from Bair Mare, Romania, measurement taken from 30 Sept. to Oct. 03, 2017; c) backward run from Kuwait City, measurement taken during Oct. 04, 2017. Result valid on 24 Sept. 2017, 0 h.

2.2. Solution of adjoint equations with RODOS MATCH

For the efficient solution of the minimisation problem (1), one has to evaluate concentrations at the locations and times of measurements c_m for arbitrary values of vector ψ. Theoretically, this could be achieved by solving a forward model, but practically, such approach is unrealistic. Another widely used method is to solve adjoint equations to establish the so-called 'source receptor function' (Marchuk, 1996). Although the RODOS system user cannot modify the source code of the MATCH model, one can still find a way to solve adjoint equations. Let us consider the Eulerian transport equation in a simplified form:

$$\partial c / \partial t + \partial(uc) / \partial x + \partial(vc) / \partial y + \partial(wc) / \partial z + Diff(c) + Decay(c) = q(x, y, z, t). \quad (2)$$

Here (u, v, w) are wind velocity components provided by numerical weather prediction (NWP) model, $Diff(c)$ is a three-dimensional diffusion operator, $Decay(c)$ describes radioactive decay, dry and wet deposition, q [Bq·m^{-3}·s^{-1}] is volumetric density distribution of source rates. Equation (2) is assumed to be solved in a spatial domain Ω on a time interval $(0, T)$.

If the nth component of the model-vector c_m is defined at the location of the nth measurement $(x_{o,n}, y_{o,n}, z_{o,n})$ and the time interval of the nth

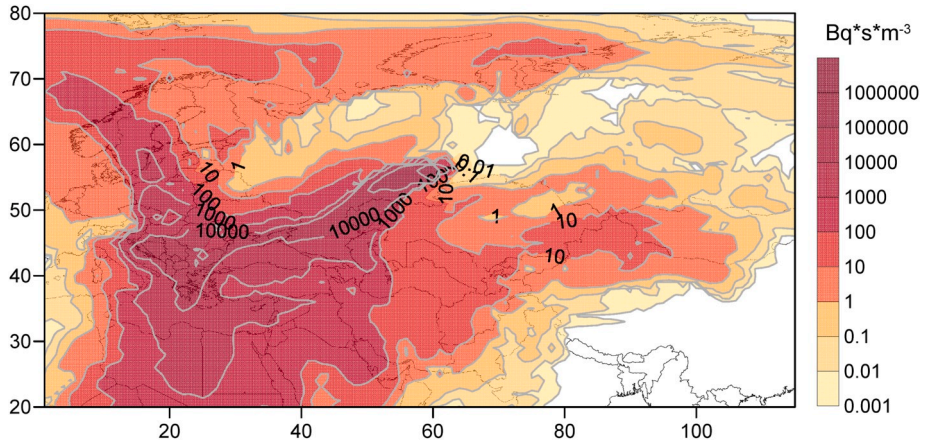

Fig. 4. Spatial distribution of time-integrated concentration following hypothetical release of 300 TBq of Ru-106 from Mayak starting on Sep. 24, 2017, 12 UTC and lasting 48 h. Result valid on Oct 08, 2017, 00 UTC.

measurement $(t_{o,n}, t_{o,n} + \delta t_{o,n})$, it can be shown (Pudykiewicz, 1998) that the solution of adjoint equation

$$-\partial c_n^*/\partial t - \partial\left(uc_n^*\right)/\partial x - \partial\left(vc_n^*\right)/\partial y - \partial\left(wc_n^*\right)/\partial z + Diff\left(c_n^*\right) + Decay\left(c_n^*\right) = p_n, \tag{3}$$

when integrated backward in time from $t = t_{o,n} + \delta t_{o,n}$ to $t = 0$, will result in the following important relationship:

$$c_m(n) = \iiint_{\Omega} \int_0^{t_{o,n}+\delta t_{o,n}} c^* \cdot q \cdot dxdydzdt, \tag{4}$$

provided that, in equation (3), p_n is the so-called 'probing function', with which the nth component of the model-vector (to be compared with the nth measurement) is formally defined through the equation

$$c_m(n) = \iiint_{\Omega} \int_{t_{o,n}}^{t_{o,n}+\delta t_{o,n}} c \cdot p_n dxdydzdt. \tag{5}$$

For instantaneous point measurement (when $\delta t_{o,n} = 0$), p_n is a product of delta-functions: $p_n = \delta(x - x_{o,n})\delta(y - y_{o,n})\delta(z - z_{o,n})\delta(t - t_{o,n})$.

Note that the diffusion operator in equation (2) is self-adjoint. Therefore, in an adjoint equation it has the same form as in the original equation. The same is true for the decay operator describing radioactive decay and wet deposition, since it has the form of: $Decay(c) = \chi c$, where χ is a coefficient describing both radioactive decay and wet scavenging and therefore depending on the precipitation rate, but not depending on c, the operator remaining linear. The above form of operator is also self-adjoint, therefore, in an adjoint equation, the operator is the same and the value of this coefficient (and hence, precipitation rate) does not have to change the sign. Finally, dry deposition is described using boundary condition at a solid boundary as follows: $K_z \partial c/\partial z|_{z=z_B} = v_d c$, where K_z is the eddy diffusivity, z_B denotes bottom boundary, and v_d is the dry deposition velocity. As it was demonstrated by Pudykiewicz (1998), in adjoint equation (2), exactly the same boundary condition, but for the adjoint variable, should be used and the sign of the dry deposition velocity does not change either. Therefore, adjoint equation (3) in this work is solved with exactly the same dry deposition velocities and scavenging coefficients as in the forward equation.

In an important case of a point source with coordinates (x_s, y_s, z_s) and a constant release rate q_s within time interval $(t_s, t_s + \delta_s)$ and zero otherwise, the spatial distribution $q(x, y, z, t)$ is given by multiplication of q_s by delta-functions that define the point source location. In this case, the following equation can be easily verified using the relationships presented above:

$$c_m(n) = q_s \int_{t_s}^{t_s+\delta t_s} c^*(x_s, y_s, z_s, t) \cdot dt. \tag{6}$$

Let us describe how we solve equation (3) using the RODOS system. The MATCH model is driven by NWP meteorological fields calculated for the simulation time interval $(0, T)$. The meteorological fields calculated on a grid are stored in files in GRIB format, each file representing a specific time $t_k : 0 \le t_k \le T$, the number of times being $K : 1 \le k \le K$. Let us denote an NWP file storing meteorological data for the kth time layer NWP_k. From the set of original NWP files NWP_k, $1 \le k \le K$, we create a new modified set of NWP files $N\tilde{W}P_m$, $1 \le m \le K$ by: 1) changing signs of the velocity components in each kth NWP file: $\tilde{u} = -u, \tilde{v} = -v$ and 2) redefining the order of files by changing indices: $m = K - k + 1$. For example, NWP_1 file containing meteorological fields for the time $t = 0$ will, after reversing velocity components, become $N\tilde{W}P_K$ file representing meteorological fields for $t = T$ and so on.

Then, we will also redefine the time variable by substitute: $\tilde{t} = T - t$, so that $\tilde{t} = 0$ when $t = T$. The solution of forward equation (1) with $\tilde{t}$ instead of t, with the reversed $(\tilde{u}, \tilde{v}, \tilde{w})$ from the modified $N\tilde{W}P$ meteorological data set and with $p_n(x, y, z, \tilde{t})$ in r.h.s instead of q, will give solution of adjoint equation (3). In practice, this means that we first prepare a new $N\tilde{W}P$ set of meteorological data with reversed velocity components and with reordered dates of files as described in the previous paragraph; then we initialise a normal run of the RODOS MATCH model with the constant source term p_n in the place of the nth measurement during the corresponding time interval: $T - t_s - \delta_s \le \tilde{t} \le T - t_s$. Note that w velocity component is calculated by MATCH internally and its reversion should be automatically rendered following reversion of horizontal wind components due to continuity equation. Concentration obtained in such run will be adjoint variable resulting from solution of equation (3).

2.3. Details of the source-inversion algorithm

Even with an efficient way of evaluating cost function J for an arbitrary value of the control vector ψ by solving adjoint equations and using equation (6), it may be very difficult to find an exact minimum of J not only because of time limitations, but also because of the non-convex nature of the cost function, such that the minimisation problem may be ill-posed. For a practical application, instead of evaluating elements of the control vector ψ in continuous space we discretise them in the following way. The set of possible solutions for a source location (x_s, y_s) is limited to the locations of the grid nodes of the MATCH model. Possible start times of the release t_s are assumed to be located within

time interval $(t_s^{\min}, t_s^{\max})$, with $t_s^{\min}, t_s^{\max}$ being input parameters. Furthermore, this interval is discretised onto N_t subintervals with a constant time step $\tau = (t_s^{\max} - t_s^{\min})/N_t$ and t_s is assumed to coincide with one of the values $t_s \in \{t_s^{\min}, t_s^{\min} + \tau, \ldots, t_s^{\min} + k\tau, \ldots, t_s^{\max}\}$, the integer index k spanning values $1 < k < N_t$. The last element of the control vector - the release interval δ_s is also discretised and is assumed to belong to one of the values $\delta_s \in \{\delta_s^1, \ldots, \delta_s^{N_\delta}\}$, where $\delta_s^1, \ldots, \delta_s^{N_\delta}$ are input parameters. When the problem becomes fully discretised the minimisation is performed with the direct method, which is a slightly adapted version of the method published by Kovalets et al. (2018). Details of this method applied in this work are provided in Supplement 1 to this paper.

3. Results of application to the Ru-106 accident

3.1. Measurements

A comprehensive review of the chronology of the event and of the communications reporting detections of Ru-106 in 2017 is described by Masson et al. (2019). Starting from October 1, 2017, different countries reported measurements of airborne concentrations of Ru-106 to IAEA (IAEA, 2017). Masson et al. (2019) published many of those and other measurements (more than 1000 values). The detected concentrations of Ru-106 varied from the lower detectable limit ($10^{-6} - 10^{-5}$ Bq·m^{-3}, depending on specific measurement) to 0.176 Bq·m^{-3} reached in Romania. The sampling times varied from 12 h to 2 weeks. Because the presented solution of adjoint equation is not automated in RODOS, requiring manual input to run the MATCH model, and because we are primarily interested in applying the method during an accident when a full set of measurements is not available, we used 118 measurements taken in locations shown in Fig. 1 that were available to the authors during the accident. Majority of the measurements used in this study are already published by Masson et al. (2019). In this paper, we also used additional measurements from Ukrainian NPPs, Roshydromet reports (Roshydromet, 2017a,b) and data from Comprehensive Nuclear-Test-Ban Treaty Organization (CTBTO) requested by Ukraine and made available to the authors of this paper (some of them were published in Ramebäck et al., 2018).

Sampling periods of the measurements used in simulations varied from 1 day (24 h) to 14 days, about 50% of the measurements had a sampling period of 1 day, and 91% of the measurements had a sampling period ≤7 days. Only 2 measurements had a sampling period of 14 days – in Sarajevo (Bosnia and Herzegovina) and Smolensk (Russia). We used those measurements as well because they represented the only available data on a territory of more than $5{\cdot}10^4$ km^2.

It should also be noted that in this work we used so-called 'zero-measurements', i.e. the measurements of less than the lower detectable limit (LDL). When the LDL was known, we set the respective measurement value equal to the LDL. However, when the LDL was not reported, we used the value of $1{\cdot}10^{-6}$ Bq·m^{-3}, which is of the order of the smallest LDL values presented in (Masson et al., 2019). A full list of measurements used in this study, together with their sampling periods and the LDL values, is provided in Supplement 2 to this paper.

3.2. Model setup and results

For the analysis of possible sources of Ru-106, we selected the following specific values for the parameters mentioned in the previous section. The total simulation period corresponding to time interval $(0, T)$ mentioned above was from 24 Sept. 2017, 00 UTC to Oct. 08, 2017, 00 UTC. The start time of the release was assumed to fall within time interval from 24 Sept. 2017, to Oct. 01, 2017, when the first detections of Ru-106 were reported. The time step τ with which this time interval was discretised (see also section 2.3) was set to 3 h. Possible durations of the release δ_s for which cost function (1) was analysed where 3, 6, 12, 24 and 48 h. The source location was assumed to fall within the domain extending from 2° to 90° E and from 20° to 80° N. The GFS Final Analysis data (NCEP, 2000) with 1 dec. deg. grid resolution was used in this study, therefore, the grid resolution of the MATCH model was the same. As it was discussed above, the source location was assumed to coincide with one of the grid nodes of the model.

The spatial distribution of maximum correlation between simulated and observed Ru-106 concentrations with a potential source located at different grid nodes is shown in Fig. 2. The region of high values of correlation function is very large; qualitatively, it is similar to the distribution of the reduction factor of the cost function presented by Saunier et al. (2019). This region is centered on the Ural Mountains; this is explained by a very wide expansion of the plume. As it is shown in Fig. 3, possible regions from which the cloud could come to Peleduj in the most eastern part of Russia, Kuwait and Europe, all intersect in the middle part of Russia.

The position of maximum correlation is shown in Fig. 2. It is located in the northern part of Russia, between the Ural Mountains and the Timan Ridge. However, there are no known nuclear installations in this region. Locations of some possible sources are shown in Fig. 2: the Mayak nuclear fuel reprocessing plant in Ozersk, Chelyabinsk region, the Research Institute of Atomic Reactors in Dimitrovgrad, Chelyabinsk region and a nuclear test site on Novaya Zemlya. Note that among these possible sources, Novaya Zemlya is located in the region of the maximum correlations (more than 0.7). Bearing in mind that Ru-106 can be used in a radioisotope generator and recalling failed military tests in this region in 2017 (The Barents Observer, 2018), this source cannot be completely excluded.

However, the most probable source according to several investigations (Masson et al., 2019; Saunier et al., 2019, Cartlidge, 2018) is the Mayak reprocessing plant in Chelyabinsk region, Russia. In Fig. 2, it is located very close to the 0.5 isoline of the correlation coefficient.

The forward simulation of dispersion following a hypothetical release from the Mayak starting on Oct. 24, 2017, 12:00 UTC and lasting 12 h indeed gives the correlation coefficient between simulated results and measurements of 0.49. However, an average inventory of such release resulting in the same average simulated concentrations as those of the measurements (5.6 mBq·m^{-3}) is very high: 4PBq. If, however, we increase the assumed duration of the hypothetical release from Mayak to 48 h, the inventory giving the same average value of concentrations as that of the measurements will decrease down to 300 TBq, which is very close to estimates by Saunier et al. (2019). The normalised mean squared error between simulated results and the measurements $NMSE = 11$. This value of *NMSE* is within the range of performances of different models in studies on long range dispersion during ETEX experiment (see for example Bellasio et al., 2012). Taking into account that uncertainties in the source term estimation in this work are combined with uncertainties in the meteorological data, this value of *NMSE* can be considered satisfactory.

Fig. 4 shows time-integrated concentration through the time period of 24 Sept. 2017–Oct. 08, 2017 calculated following a hypothetical release from Mayak starting on Oct. 24, 2017, 12:00 UTC and lasting 48 h. The plume is first transported southwest and near western border of Kazakhstan is split into two parts. The first part of the plume follows the anticyclonic circulation and moves along southern border of Russia to the Far East (Fig. 2-a). The second part of the plume is further transported to the South-West and is in turn split into two parts: one is transported to Europe (Fig. 2-b) and the other to the South to reach Kuwait (Fig. 2-c).

4. Discussion and Conclusions

In this work, we developed and presented a method to use the European nuclear emergency response system RODOS for analysis of potential sources of radioactivity of an unknown origin. The method is based on solving the adjoint equations. It does not require modification of the code of the long-range atmospheric dispersion model MATCH

used in RODOS. Instead, a solution of the adjoint equation is calculated in the forward version of the model by reversing velocity components in the input files and reordering dates. At the present stage, the method is not automated and requires manual initialisation of backward runs. However, the method was successfully applied to the Ru-106 accident of 2017. Preliminary results obtained with this method were among the first published in the Internet.

The application of the method to the Ru-106 accident presented in this paper shows that the spatial distribution of the correlation between simulations and measurements given the location source, is in a qualitative agreement with analogous results published elsewhere, such as the spatial distribution of the reduction factor presented by Saunier et al. (2019). The region of high correlation is centered on the Ural Mountains; this is explained by a very wide expansion of the plume. However, the location of maximum correlation obtained in this work is in the northern part of Russia, close to a military test site on Novaya Zemlya. This location is far away from the reprocessing plant Mayak in the South-Eastern Urals mentioned in other investigations as the most probable location of the source. However the hypothesis of release at military test site on Novaya Zemlya is in line with some other studies, such as Mietelski and Povinec (2020) who considered hypothesis of the Ru-106 release in a nuclear jet engine test. In the results presented here, the correlation at the source location corresponding to the Mayak plant is still quite high (0.49) and release inventory from this source of about 300 TBq could explain the observed measurements. The method can be further improved by taking into consideration time variability of the release. However, for real-time screening assessments during an accident, this method is a suitable tool allowing RODOS users to analyse potential sources when the release location is unknown.

Declaration of competing interest

The authors declare that they have no known competing financial interests or personal relationships that could have appeared to influence the work reported in this paper.

Acknowledgements

We thank the State Nuclear Inspectorate of Ukraine for providing CTBTO measurements. This work was supported by funding from the National Academy of Sciences of Ukraine and Kyiv Academic University (registration numbers of projects 0119U001433 and 0120U101734). We thank three anonymous reviewers and Oleksiy Danylenko for their valuable comments.

Appendix A. Supplementary data

Supplementary data to this article can be found online at https://doi.org/10.1016/j.jenvrad.2020.106302.

References

Hamburger, T., Gering, F., 2019. Assessment of source regions and source terms based on the Ru-106 measurements in air in Europe in September and October 2017, 19th International Conference on Harmonisation within Atmospheric Dispersion Modelling for Regulatory Purposes. Harmo 2019.

Bellasio, R., Scarpato, S., Bianconi, R., Zeppa, P., 2012. APOLLO2, a new long range Lagrangian particle dispersion model and its evaluation against the first ETEX tracer release. Atmos. Environ. 57, 244–256. https://doi.org/10.1016/j.atmosenv.2012.04.017.

Bossew, P., Gering, F., Petermann, E., Hamburger, T., Katzlberger, C., Hernandez-Ceballos, M.A., De Cort, M., Gorzkiewicz, K., Kierepko, R., Mietelski, J.W., 2019. An episode of Ru-106 in air over Europe, September–October 2017 – geographical distribution of inhalation dose over Europe. J. Environ. Radioact. ISSN: 0265-931X 205–206, 79–92. https://doi.org/10.1016/j.jenvrad.2019.05.004, 2019.

Cartlidge, E., 2018. Isotope cloud linked to failed neutrino source. Science 359, 729, 2018.

Enting, I.G., 2002. Inverse Problems in Atmospheric Constituent Transport. Cambridge University Press, Cambridge, 2002.

IAEA, 2017. Updated technical attachment status of measurements of Ru-106 in Europe, 2017-10-20. Prepared by the incident and emergency centre of the IAEA. Available online. https://www.criirad.org/accident-et-pollutions/aiea_Ru-106_Technical_Attachment-2.pdf. Accessed 3 March 2020.

Ievdin, I., Trybushny, D., Zheleznyak, M., Raskob, W., 2010. RODOS re-engineering: aims and implementation details. Radioprotection 45 (5), S181–S189. https://doi.org/10.1051/radiopro/2010024.

Kovalets, I., 2017. Where is the source of ruthenium-106? https://www.linkedin.com/pulse/potential-sources-ruthenium-ivan-kovalets/. Accessed 3 March 2020.

Kovalets, I.V., Romanenko, A.N., 2017. Detection of ruthenium-106 in 2017: meteorological analysis of the potential sources. https://www.linkedin.com/pulse/detection-ruthenium-106-2017-meteorological-analysis-sources-ivan/. Accessed 3 March 2020.

Kovalets, I.V., Robertson, L., Persson, C., Didkivska, S.N., Ievdin, I.A., Trybushnyi, D., 2014. Calculation of the far range atmospheric transport of radionuclides after the Fukushima accident with the atmospheric dispersion model MATCH of the JRODOS system. Int. J. Environ. Pollut. 54 (2/3/4), 101–109. https://doi.org/10.1504/IJEP.2014.065110, 2014.

Kovalets, I.V., Efthimiou, G.C., Venetsanos, A.G., Andronopoulos, S., Kakosimos, E.K., Argyropoulos, D.C., 2018. Inverse identification of an unknown finite-duration air pollutant release from a point source in urban environment. Atmos. Environ. 181, 82–96. https://doi.org/10.1016/j.atmosenv.2018.03.028.

Landman, C., Päsler-Sauer, J., Raskob, W., 2014a. The decision support system RODOS. In: The Risks of Nuclear Energy Technology. Science Policy Reports. Springer, Berlin, Heidelberg. https://doi.org/10.1007/978-3-642-55116-1_21.

Landman, C., Päsler-Sauer, J., Raskob, W., 2014b. RODOS and the Fukushima accident. In: The Risks of Nuclear Energy Technology. Science Policy Reports. Springer, Berlin, Heidelberg. https://doi.org/10.1007/978-3-642-55116-1_22.

Marchuk, G., 1996. Adjoint Equations and Analysis of Complex Systems. Kluwer Academic Publishers, Dodrecht, Netherlands.

Masson, O., Steinhauser, G., Zok, D., Saunier, O., et al., 2019. Airborne concentrations and chemical considerations of radioactive ruthenium from an undeclared major nuclear release in 2017. Proc. Nat. Acad. Sci. 116 (34), 16750–16759. https://doi.org/10.1073/pnas.1907571116. Aug 2019.

Mietelski, J.W., Povinec, P.P., 2020. Environmental radioactivity aspects of recent nuclear accidents associated with undeclared nuclear activities and suggestion for new monitoring strategies. J. Environ. Radioact. (214–215), 106151. https://doi.org/10.1016/j.jenvrad.2019.106151.

NCEP, 2000. National Centers for Environmental Prediction/National Weather Service/NOAA/U.S. Department of Commerce, 2000: NCEP FNL Operational Model Global Tropospheric Analyses, Continuing from July 1999. Research Data Archive at the National Center for Atmospheric Research, Computational and Information Systems Laboratory. Boulder, CO. http://rda.ucar.edu/datasets/ds083.2. Accessed 03 March 2020.

Pudykiewicz, J., 1998. Application of adjoint tracer transport equations for evaluating source parameters. Atmos. Environ. 32, 3039–3050.

Ramebäck, H., Söderström, C., Granström, M., Jonsson, S., Kastlander, J., Nylén, T., Ågren, G., 2018. Measurements of 106Ru in Sweden during the autumn 2017: gamma-ray spectrometric measurements of air filters, precipitation and soil samples, and in situ gamma-ray spectrometry measurement. Appl. Radiat. Isot. 140, 179–184. https://doi.org/10.1016/j.apradiso.2018.07.008.

Robertson, L., 2010. MATCH development during the EURANOS project. Radioprotection 45, S85–S88.

Robertson, L., Langner, J., 1999. An Eulerian limited area atmospheric transport model. J. Appl. Meteorol. 38, 190–210.

Roshydromet, 2017. Bulletin on radiation situation in Russia in October, 2017 (Бюллетень о радиационной обстановка на территории России в Октябре 2017) [in Russian]. http://www.criirad.org/accident-et-pollutions/byulleten-rorf-10-2017.pdf. Accessed 3 March 2020.

Roshydromet, 2017. Report on the causes and source of ruthenium in Russia in September-October 2017 (Отчет по определению причин и источника рутения в России в сентябре-октябре 2017) [in Russian]. http://egasmro.ru/files/documents/reports/report_28_12_2017.pdf. Accessed 3 March 2020.

Saunier, O., Didier, D., Mathieu, A., Masson, O., Dumont Le Brazidec, J., 2019. Atmospheric modeling and source reconstruction of radioactive ruthenium from an undeclared major release in 2017. Proc. Natl. Acad. Sci. Unit. States Am. 116 (50), 24991–25000. https://doi.org/10.1073/pnas.1907823116. Dec 2019.

Sørensen, J.H., 2018. Method for source localization proposed and applied to the October 2017 case of atmospheric dispersion of Ru-106. J. Environ. Radioact. 189, 221–226. https://doi.org/10.1016/j.jenvrad.2018.03.010.

The Barents Observer, 2018. Nuclear-powered missile crashed in Barents Sea, intelligence report allegedly claims, 22 August, 2018, Available online. https://thebarentsobserver.com/en/security/2018/08/nuclear-powered-missile-crashed-barents-sea-intelligence-report-allegedly-claims. Accessed 3 March 2020.